Thermally evaporated Ag nanoparticle films for plasmonic enhancement in organic solar cells: effects of particle geometry

Haidari, G.; Hajimahmoodzadeh, M.; Fallah, H.R.; Peukert, A.; Chanaewa, A.; von Hauff, E.L.

published in
Physica Status Solidi. Rapid Research Letters
2015

DOI (link to publisher)
10.1002/pssr.201409528

document version
Publisher's PDF, also known as Version of record

Phys. Status Solidi RRL **9**, No. 3, 161–165 (2015) / **DOI** 10.1002/pssr.201409528

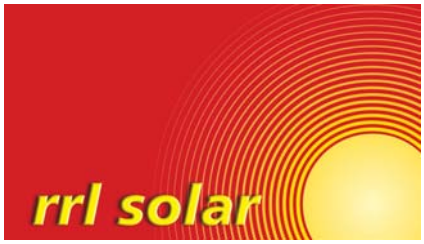

Thermally evaporated Ag nanoparticle films for plasmonic enhancement in organic solar cells: effects of particle geometry

Gholamhosain Haidari[*,1], Morteza Hajimahmoodzadeh[1,2], Hamid Reza Fallah[1,2], Andreas Peukert[3], Alina Chanaewa[3], and Elizabeth von Hauff[3,4]

[1] Department of Physics, University of Isfahan, P.O. Box 81746-7344, Isfahan, Iran
[2] Quantum Optics Research Group, University of Isfahan, Isfahan, Iran
[3] Institute of Physics, University of Freiburg, Freiburg, Germany
[4] Physics of Energy, Department of Physics and Astronomy, Vrije University Amsterdam, Amsterdam, Netherlands

Received 30 November 2014, revised 5 January 2015, accepted 3 February 2015
Published online 9 February 2015

Keywords Ag nanoparticles, plasmonics, organic solar cells, low band gap polymer, optical simulation

[*] Corresponding author: e-mail moh1135@gmail.com, Phone: +983137934728, Fax: +983137932409

We report on the simple fabrication of Ag NP films via thermal evaporation and subsequent annealing. The NPs are formed on indium tin oxide electrodes, coated with PEDOT:PSS and implemented into PCPDTBT:PC70BM solar cells. Scanning electron microscopy and atomic force microscopy are used to determine the size distributions and surface coverage of the NP film. We apply finite-difference time-domain techniques to model the optical properties of different nanoparticle films and compare this with the absorption properties of the organic active layer. The simulations demonstrate that the absorption and scattering efficiency of the particles are very sensitive to particle geometry. Solar cells prepared with window electrodes containing NP layers with less surface coverage, show a 14.8% improvement in efficiency. We discuss variations in the external quantum efficiency of the devices in terms of forward scattering and parasitic absorption losses induced by the NP layer.

1 Introduction Organic photovoltaic (OPV) devices are of great interest due to their potential as a low cost, high throughput, and flexible source of clean energy. For OPV to become commercially viable, however, the power conversion efficiency must be improved further. Low carrier mobility combined with the large band gap of organic semiconductors pose a critical barrier for the photocurrents, and therefore the efficiencies, of these devices [1, 2].

Currently, high efficiencies have been reported for polymer:fullerene solar cells based on low band gap polymers, such PCPDTBT [2]. These polymers have increased light harvesting properties due to their energetically smaller band gaps. However, films of low band gap polymers also have characteristically high electronic disorder leading to low carrier mobility, so that only very thin layers can be applied ultimately limiting light absorption in the device.

Several approaches have been investigated to further increase light harvesting in the organic photoactive layer. The most commonly investigated strategies include the implementation of an inorganic optical spacer [3] between the active layer and metal electrodes, and the incorporation of plasmonic structures [4–7].

The hybrid nature of surface plasmon (SP) modes, propagating surface plasmon polaritons (SPPs) and localized surface plasmons (LSPs), make plasmonic materials attractive candidates for a variety of energy applications [8]. The use of metal nanoparticles (MNPs) or nanoclusters [9–12] with plasmonic resonance in the visible range is promising for increasing the optical absorption of solar cells via enhanced scattering and coupling of incident light into the active layer as well as light confinement around the NP surface. In addition, the easy tunability of the NPs' optical properties by modifying size, shape and surrounding materials [13, 14] can be taken advantage of as a tool

for optical engineering photonic devices. Silver and gold NPs are commonly employed as their plasmon resonance effects are well suited for photovoltaics [15]. The plasmon excitation of silver nanoparticles is known to be more pronounced than that of gold resulting in stronger, sharper plasmon resonance peaks [15].

Incorporation of MNPs in the buffer PEDOT:PSS layer of OPV is one of the simpler methods to take advantage of plasmonic effects [5, 9, 13]. Despite substantial research activities on this topic, studies are missing which apply both simulation and experimental tools to reveal deeper insight into mechanisms leading to increases in photocurrent and power conversion efficiency [9, 16]. Besides beneficial effects for light absorption, mechanisms such as charging, recombination and parasitic absorption by MNPs can lead to significant losses in OPV [15]. Therefore, deeper insight into how MNPs influence the optical properties of OSCs is required.

We fabricate Ag NP layers on indium tin oxide (ITO) electrodes via thermal evaporation and subsequent annealing. The NP films are implemented into PCPDTBT:PC70BM solar cells. Scanning electron microscopy (SEM) and atomic force microscopy (AFM) are used to characterize the geometry and surface coverage of the NP films. The absorption and scattering efficiencies of the particles were modelled using Finite-difference time-domain (FDTD) techniques. We discuss the external quantum efficiency (EQE) spectra of the solar cells in terms of the absorption and scattering efficiency of the NPs.

2 Experimental method

2.1 Device fabrication ITO coated glass slides were cleaned with soap and water and sequentially ultrasonicated for 10 min in deionized water, acetone and isopropanol alcohol and dried with nitrogen. Ag NP films were fabricated via thermal deposition on ITO substrates at a rate of 0.2 A/s at a pressure of 8×10^{-7} mbar, followed by annealing at 200 °C for 15 min under nitrogen. Ag film thicknesses of 2 nm and 5 nm were chosen as they were sufficiently thin to be below the percolation limit [17] as well as allow light to reach the active layer. The Ag film thickness was monitored using a quartz crystal oscillator inside the chamber. 40 nm of PEDOT:PSS (Clevios AI 4083 filtered with a 0.45 μm PTFE syringe filter) was spin cast on thin Ag films, followed by annealing in nitrogen at 180 °C for 10 min.

The solar cell active layer was prepared from solutions containing 1:3.6 blend ratios (by weight) of PCPDTBT and PC70BM. 1,2-dichlorobenzene was used as the solvent processed with 2.5 vol% 1,8-octanedithiol as the additive. The total blend concentration was 36 mg/ml and spin coating was performed at 1400 rpm for 40 sec resulting in an active layer thickness of ~110 nm [18]. The solar cells were contacted by thermally evaporating 30 nm Ca and 100 nm Al with a base pressure below 10^{-6} mbar through a shadow masks, resulting in an active area of 0.263 cm^2. Devices were encapsulated with epoxy resin in the glove box before measurement.

2.2 Characterization Atomic force microscopy (AFM-NanoscopeIIIa Digital Instrments,Veeco), scanning electron microscopy(SEM-Quanta 250 FEG by company FEI), transmission spectra, current density–voltage (J–V) characteristics and EQE measurements were performed on samples at room temperature. The current–voltage characteristics were obtained with a Keithley 2400 source meter under 100 mW/cm^2 using a solar simulator (500 W Oriel lamp calibrated with solar reference Si cell certified by Fraunhofer ISE). Absorption and EQE spectra were measured using a home-made setup consisting of an Oriel lamp, monochromator Omni 150, detectors and a Keithley 2400.

3 Results and discussion Ag deposited on glass/ITO forms ultra-thin discontinuous films, corresponding to Volmer–Weber growth [19]. After annealing the film consists of regularly shaped and sized particles or nanoclusters with reduced surface coverage. We prepared thin Ag films with initial thicknesses of 2 nm and 5 nm. Absorption

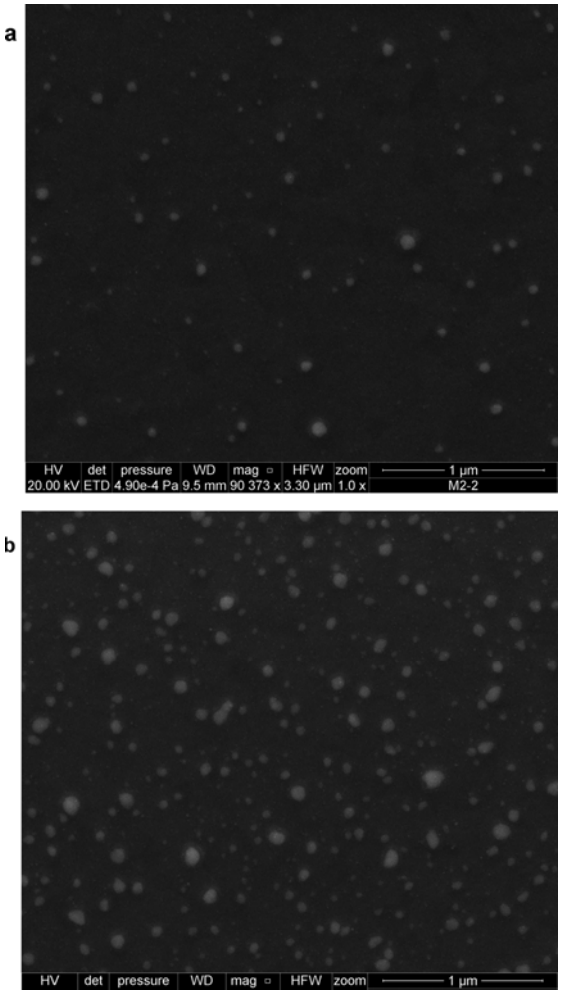

Figure 1 (a) SEM images of sample A and (b) sample B.

measurements were used to confirm the formation of particles after annealing (see Supporting Information, Table S1 and Fig. S2). Figure 1(a, b) shows SEM images of the annealed Ag NP films (2 nm and 5 nm). We will refer to these as sample A and B, respectively. In both samples Ag NPs are embedded in PEDOT:PSS, and a high voltage of 20 kV was applied to deliberately discriminate between the MNP and the polymer layer.

The mean $R_{\|}$ and standard deviation of Ag NPs are 21.93 nm and 1933.24 nm for sample A as well as 27 nm and 2693.978 nm for sample B, respectively (see Supporting Information, Figs. S3–S6 and Tables S2 and S3).

Differences in size and geometry of the NPs are expected to have an impact on the optical properties, as the NPs not only absorb the incident light, but also scatter anisotropically [20] depending on size and shape. In order to understand these effects we performed simulations using the FDTD method with a freely available software package, meep [21]. With this technique the spatial and temporal variations in the electromagnetic field can be obtained by rigorously solving Maxwell's equations. The simulation zone consists of a three dimensional separated truncated spheroid Ag particle at interface between ITO and PEDOT:PSS. Perfectly matched layers (PML) boundary conditions were used along all directions. The light source is a Gaussian-pulse source, which travels along the y-direction and is polarized along the x-direction. The Lorentz–Drude values for Ag were taken from [22].

The structure of the computational domain is shown schematically in the inset of Fig. S1 in the Supporting Information. The particle height (H) was fixed at 34.5 nm (sample A) and 22.8 nm (sample B), respectively. This leads to more prolate particles in the case of sample A, and more oblate particles in the case of sample B. To account for the distribution in particle width observed in the NP films, the parallel radius, $R_{\|}$, was varied between 10 nm and 70 nm.

The scattering and absorption efficiencies of the samples A and B are shown in Fig. 2(a, b) and 2(c, d), respectively (see also Supporting Information, Section 5 for more information and additional FDTD simulations). Similar efficiencies for 2D periodic NPs in the complete structure of solar cell are presented in Fig. S12(a), b).

The simulation results show that maximum absorption efficiency occurs for $R_{\|} = 30$ nm. Moreover, the resonance peak broadens and shifts to longer wavelengths with increasing $R_{\|}$. For $R_{\|} > 30$ nm, absorption efficiency decreases in favour of scattering, until a maximum (forward) scattering efficiency occurs at $R_{\|} = 50$ nm. For this value, scattering for prolate spheroids (sample A) is more efficient than that of oblate spheroids (sample B) in the spectral regime where PCPDTBT absorbs.

While scattering efficiency is sensitive to particle size and geometry, we find that near field effects on polymer absorption are negligible (see Supporting Information, Fig. S13). The electric field profile is found to distribute laterally rather than normal to the substrate. As the parti-

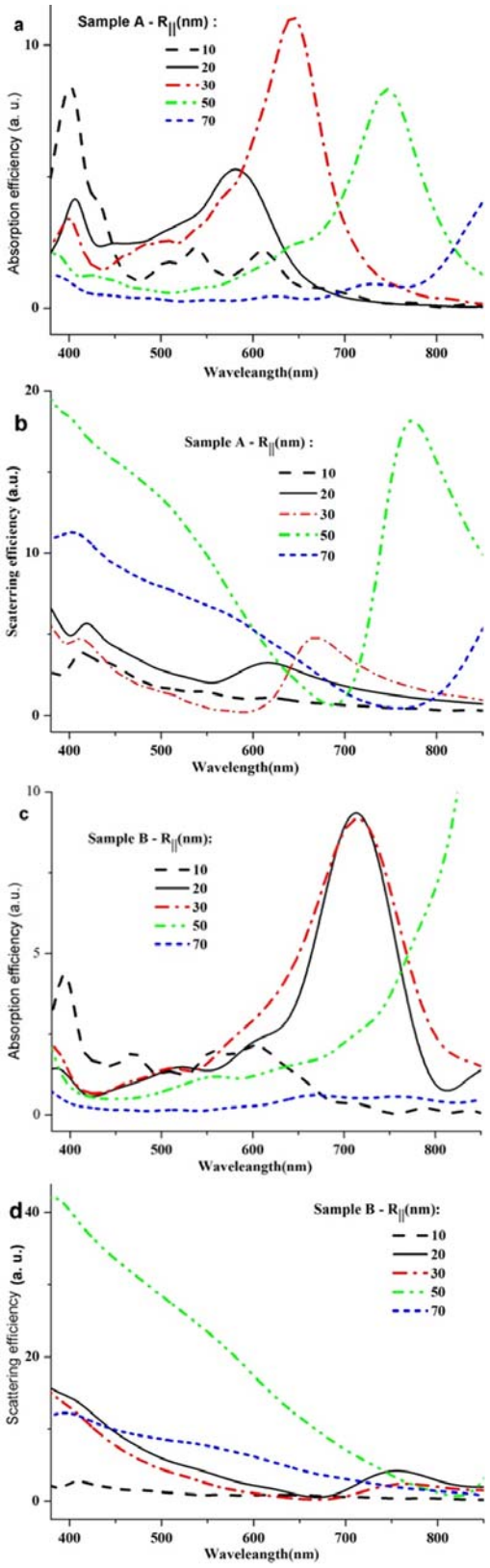

Figure 2 FDTD absorption and scattering efficiencies of truncated prolate spheroid Ag (sample A) (a, b) and truncated oblate spheroid Ag (sample B) (c, d).

Table 1 Device performance of PCPDTBT:PC70BM solar cells with and without Ag NPs, recorded under illumination at 100 mW/cm^2 (see Supporting Information, Fig. S14 for dark J–V characteristics).

sample no.	V_{oc} (V)	J_{sc} (mA/cm^2)	FF	PCE (%)
solar cell with no Ag NPs	0.61	9.1	0.40	2.22
solar cell with A anode	0.62	10.0	0.41	2.55
solar cell with B anode	0.60	8.8	0.40	2.11

cles are embedded in PEDOT:PSS the electric field arising from the NP does not extend into the active layer.

Finally we investigated the influence of the Ag NP films on the performance of PCPDTBT:PC70BM solar cells. The blend has absorption maxima at ~420 nm, ~560 nm, ~760 nm and ~800 nm (inset of Fig. 3). Both PCPDTBT and PC70BM contribute to the absorption in the region of the ~420 nm peaks, while the peak at ~760 nm is attributed solely to PCPDTBT. The peak at ~800 nm arises due to the solvent additive 1,8-octanedithiol [23, 24]. We observe that the Ag NPs lead to variations in the short-circuit current (J_{sc}) while the open-circuit voltage (V_{oc}) and fill factor (FF) remain comparable between the devices (Table 1).

The EQE spectra of solar cells prepared with no NP (blue), sample A anode structure (black), and sample B anode structure (red) are shown in Fig. 3.

The EQE spectrum of the reference device follows the profile of the absorption spectrum of the PCPDTBT:PC70BM blend,with an additional maximum around 560 nm which can be attributed to PC70BM [23, 24].

Solar cells prepared with the sample A window anode, show an enhancement in EQE of 6% and 13% for the maxima at 560 nm and 760 nm, respectively. In contrast devices prepared with a sample B window anode demonstrate a lower EQE signal over the entire wavelength range.

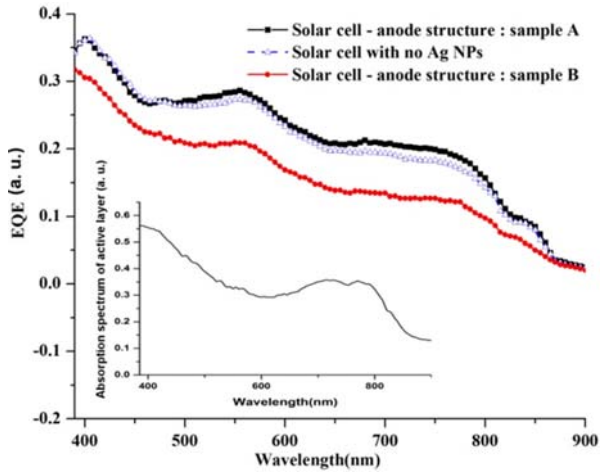

Figure 3 EQE spectra of three kinds of PCPDTBT:PC70BM devices. The inset shows the absorption spectrum of active layer.

These results demonstrate that for varied size of MNPs, plasmonic enhancement in organic solar cells depends critically on the properties, particularly shape, size distribution and number of the NPs in each range of size distribution, positioned at the anode. Although the NP films were fabricated in the same way, the initial thickness of the layer leads to variations in the shape and number of the NPs. In particular, the prolate particles, formed from thinner Ag films lead to advantageous forward scattering effects at wavelengths which are relevant for polymer absorption. The oblate particles formed from thicker Ag films, on the other hand, show decreased scattering efficiencies and increased absorption at longer wavelengths, leading to parasitic absorption losses. We find that near-field effects do not play a considerable role for this device architecture, as the electric field due to the NPs is distributed laterally and the strongest part is more close to ITO interface, thereby it does not extend from the PEDOT:PSS buffer into the active layer.

4 Conclusion We investigated the influence of Ag NP films prepared by thermal evaporation and annealing on the performance of PCPDTBT:C70BM solar cells. We prepared Ag NP films with initial thicknesses of 2 nm and 5 nm. From the SEM and AFM data we could determine the size distributions of the MNPs. Optical modelling revealed the influence of the size and geometry of the MNPs on the scattering and absorption efficiencies. From this we could attribute enhancement in the EQE data for prolate MNPs to preferential forward scattering into the active layer. On the other hand, for the oblate MNPs, decreases in EQE of the solar cell were found to be due to parasitic absorption losses because of overlap in the absorption of the MNPs and active layer.

Supporting Information Additional supporting information may be found in the online version of this article at the publisher's website.

Acknowledgements The authors would like to thank Graduate Office of University of Isfahan and International Office of Freiburg University for their support.

References

[1] O. A. Abdulrazzaq et al., Part. Sci. Technol. **31**, 427 (2013).
[2] J. You et al., Nature Commun. **4**, 1446 (2013).
[3] B. V. Andersson et al., Appl. Phys. Lett. **94**, 4 (2009).
[4] H. A. Atwater et al., Nature Mater. **9**, 205 (2010).
[5] K. R. Catchpole et al., Opt. Express **16**, 21793 (2008).
[6] S. Y. Chou et al., Opt. Express **21**, A60 (2013).
[7] X. Li et al., Appl. Phys. Lett. **102**, 153304 (2013).
[8] S. V. Boriskina et al., Mater. Today **16**, 375 (2013).
[9] D. D. S. Fung et al., J. Mater. Chem. **21**, 16349 (2011).
[10] A. P. Kulkarni et al., Nano Lett. **10**, 1501 (2010).
[11] J.-Y. Lee et al., Opt. Express **18**, 10078 (2010).
[12] D. Qu et al., Opt. Express **19**, 24795 (2011).
[13] K. Inho et al., J. Phys. D, Appl. Phys. **45**, 065101 (2012).

[14] K. L. Kelly et al., J. Phys. Chem. B **107**, 668 (2002).
[15] C. D. Geddes, Reviews in Plasmonics 2010 (Springer, 2011).
[16] R. S. Kim et al., Opt. Express **20**, 12649 (2012).
[17] F. Nehm et al., Thin Solid Films **556**, 381 (2014).
[18] S. Albrecht et al., Org. Electron. **13**, 615 (2012).
[19] H. Luth, Surface and Interfaces of Solids, Surface Science, Vol. 15 (Springer-Verlag, Berlin, 1992).
[20] S.-W. Baek et al., Sci. Rep. **3**, 1 (2013).
[21] A. F. Oskooi et al., Comp. Phys. Commun. **181**, 687 (2010).
[22] A. D. Rakic et al., Appl. Opt. **37**, 5271 (1998).
[23] J. K. Lee et al., J. Am. Chem. Soc. **130**, 3619 (2008).
[24] J. Peet et al., Nature Mater. **6**, 497 (2007).